JOURNAL OF CATALYSIS **173,** 519–529 (1998)
ARTICLE NO. CA971948

Effects of Isobutylene on Isobutane Isomerization over H-Mordenite

K. B. Fogash,[1] Z. Hong, and J. A. Dumesic[2]

Department of Chemical Engineering, University of Wisconsin, Madison, Wisconsin 53706

Received July 21, 1997; revised October 17, 1997; accepted October 22, 1997

Reaction kinetics studies were conducted of isobutane conversion over H-mordenite at 473 K using a system comprised of two reactors connected in series. The first reactor was loaded with Pt/Sn catalyst and controlled the olefin concentration in the feed to the second reactor containing H-mordenite by varying the dehydrogenation–hydrogenation equilibrium between butanes and butenes. The presence of isobutylene increases the rate of isobutane isomerization and increases the rates of side reactions such as coking and oligomerization/β-scission processes which lead to C_3, C_5, and C_6 products. The kinetic data for the production of C_3, C_4, C_5, and C_6 species were described by a kinetic model involving olefin adsorption/desorption, oligomerization/β-scission, and hydride transfer steps. The rates of oligomerization/β-scission steps involving C_4 species are faster than the rates of hydride transfer for our reaction conditions.

INTRODUCTION

The isomerization of *n*-butane has been studied extensively over solid acid catalysts. For example, unpromoted and promoted forms of sulfated zirconia have been found to be effective for *n*-butane isomerization at temperatures below 423 K (1–3). These catalysts, however, undergo rapid deactivation during *n*-butane isomerization unless hydrogen is present in the feed (4–9). Olefins have been found to act as promoters for butane conversion (9–12), but these compounds may also cause more rapid catalyst deactivation. Importantly, we have recently observed slower rates of catalyst deactivation for isobutane isomerization over both sulfated zirconia and H-mordenite compared to *n*-butane isomerization (13). This behavior of isobutane allows us to elucidate more clearly the effect of olefins on catalytic activity for isobutane isomerization over H-mordenite, where deactivation does not alter catalyst performance.

EXPERIMENTAL

The H-mordenite catalyst used in this study was prepared from Na-mordenite precursor (Mobil) by ion exchange with NH_4NO_3. The exchanged catalyst was calcined in a stream of dry oxygen at 673 K for 4 h and stored in a desiccator until further use in reaction kinetics and catalyst characterization studies. The H-mordenite catalyst has a Si/Al ratio of 17, with 0.58% Na (analyzed by Galbraith Laboratories, Inc). Microcalorimetric measurements of ammonia adsorption at 423 K indicate that this H-mordenite catalyst possesses ~400 μmol of accessible acid sites per gram of catalyst.

Reaction kinetics studies were conducted in a system of two quartz flow-reactors (1.0 cm in diameter) connected in series, which is similar to a system used by Weisz for *n*-butane conversion (11, 14). The first reactor was loaded with 0.9 g of Pt/Sn catalyst. The temperature of this reactor was changed from 523 to 623 K to control the olefin concentration in the feed to the second reactor, by varying the dehydrogenation–hydrogenation equilibrium between butanes and butenes. Isobutylene was the major olefin impurity in the isobutane feed, and most of the *n*-butenes were hydrogenated to *n*-butane over the Pt/Sn catalyst. When the temperature of Pt/Sn catalyst bed was maintained at 298 K, no olefins were detected in the effluent stream from the first reactor.

Isobutane isomerization was studied in the second reactor loaded with 0.2 g of H-mordenite catalyst. Reaction kinetics measurements were conducted at 473 K with weight-hourly space-velocities (WHSV) of isobutane (10 to 80% isobutane, AGA, 99.5% purity, instrument grade) from 4.7 to 37.3 h^{-1}, with H_2 (Liquid Carbonic, generally 10%) and He (Liquid Carbonic) as the balance for a total pressure of 1 atm. The total flow rate of feed to the catalyst was 60 cm^3(STP)/min. The H_2 and He gases were purified by an oxygen absorbent trap (Alltech), and water impurities were removed by molecular sieve traps at 77 K. Isobutane was used directly from the cylinder without further purification. The predominant impurities in the isobutane feed to the second reactor were *n*-butane (ca 2500 ppm), propane (ca 1000 ppm), and trace quantities of pentanes (ca 50 ppm). Reaction products were analyzed using a Hewlett Packard 5890 Gas Chromatograph with a flame-ionization detector. Gas separation was achieved by a packed column (0.19% picric acid on Graphpac-GC, 80/100, Alltech) with temperature programming, i.e., column held at 323 K for 5 min, then ramped to

[1] Current address: Air Products and Chemicals, Inc., 7201 Hamilton Boulevard, Allentown, PA 18195-1501.

[2] To whom correspondence should be addressed.

0021-9517/98 $25.00

TABLE 1

Reaction Conditions for Isobutane Isomerization over H-Mordenite at 473 K

Catalyst weight (gram)	Feed composition[a] (%)		Olefin level (ppm)
	i-C_4H_{10}	H_2	i-C_4H_8
0.20	12	10	55
0.20	12	10	143
0.20	12	10	224
0.20	12	10	346
0.22	10	10	78
0.22	19	10	82
0.22	49	10	78
0.22	80	10	77
0.22	10	50	76
0.22	12	10	~0

[a] Total pressure of 1 atm, with He as the balance.

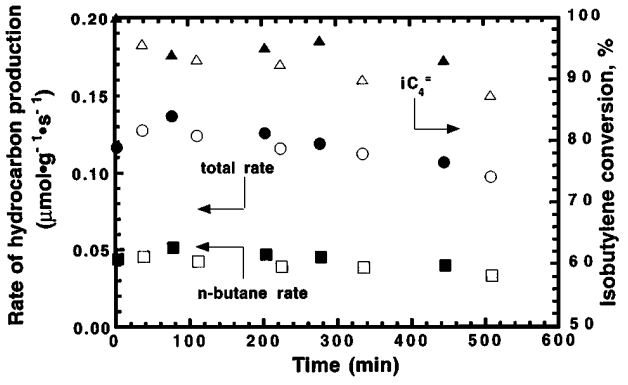

FIG. 1. Rates of hydrocarbon production and isobutylene conversion versus time-on-stream. Total hydrocarbon production for 10% H_2 (○) and 50% H_2 (●) in feed, *n*-butane production for 10% H_2 (□) and 50% H_2 (■) in feed, isobutylene conversion for 10% H_2 (△) and 50% H_2 (▲) in feed. Isobutane pressure = 0.10 atm.

373 K at 10 K/min, and held at 373 K until the analysis was complete.

The same H-mordenite catalyst was used for all kinetics studies. The catalyst was regenerated between experiments by calcination in dry O_2 at a flow rate of 60 cm^3(STP)/min at 823 K for 3 h. Tests revealed that this treatment restores the same activity for isobutane isomerization reaction as exhibited by a fresh catalyst sample for the same reaction conditions.

Table 1 presents the reaction conditions employed in this study of isobutane isomerization over H-mordenite at 473 K, where (a) the inlet olefin concentration is varied at the same isobutane concentration, (b) the inlet isobutane concentration is varied at the same olefin concentration, (c) the hydrogen concentration is changed with the same olefin and isobutane concentration, and (d) no detectable olefins are present in the feed.

RESULTS

Experimental Results

Figure 1 shows the rate of total hydrocarbon production (i.e., C_3, C_4, C_5, and C_6 hydrocarbons adjusted to reflect the amount of isobutylene converted), the rate of *n*-butane production, and the isobutylene conversion versus time-on-stream for isobutane isomerization over H-mordenite at 473 K for 10% isobutane, ~77 ppm of isobutylene, and 10% hydrogen in the feed or 50% hydrogen in the feed. The rates of hydrocarbon and *n*-butane production are approximately constant over the reaction time of 500 min, and it appears that the effect of H_2 is small under these reaction conditions. The selectivity for *n*-butane is ca 40% and does not change with time-on-stream.

Figure 2 shows the corresponding rates of production of C_3 (propane and propylene), isopentane, *n*-pentane, and C_6 for the reaction conditions of Fig. 1. This figure shows that the rate of isopentane production is about twice the rate of C_3 production. The rate of C_6 production is an order of magnitude lower than the rate of isopentane production, and very low rates of *n*-pentane production are observed (<0.001 μmol/(g·s)). The concentration of hydrogen has little effect on the rates of formation of C_3–C_6 species over H-mordenite.

Figure 3 shows the rate of total hydrocarbon production versus time-on-stream at 473 K for experiments in which the olefin concentration was varied. For inlet olefin concentrations lower than 150 ppm, little or no deactivation is observed during the reaction time (ca 250 min), while faster deactivation appears to take place for inlet olefin concentration higher than 150 ppm. In addition, an induction period is

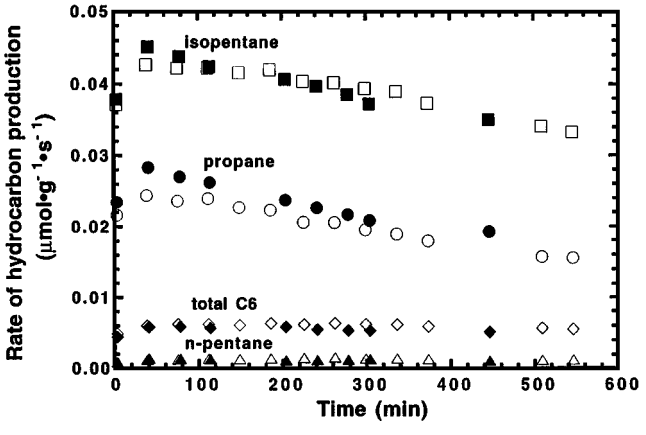

FIG. 2. Rates of hydrocarbon production versus time-on-stream. Isopentane production for 10% H_2 (□) and 50% H_2 (■) in feed, C_3 production for 10% H_2 (○) and 50% H_2 (●) in feed, *n*-pentane production for 10% H_2 (△) and 50% H_2 (▲) in feed, C_6 production for 10% H_2 (◇) and 50% H_2 (◆) in feed. Isobutane pressure = 0.10 atm.

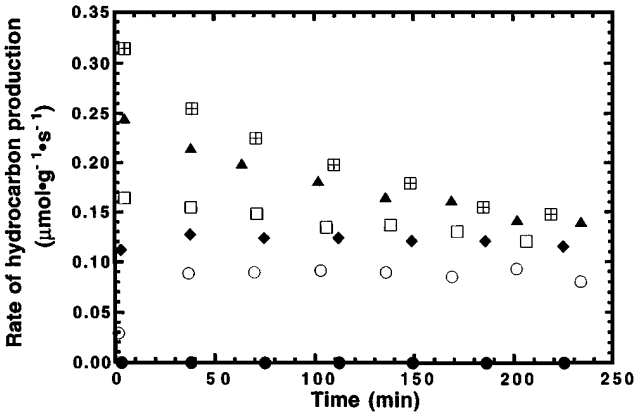

FIG. 3. Rates of total hydrocarbon production versus time-on-stream. Isobutylene levels of 346 ppm (⊞), 224 ppm (▲), 143 ppm (□), 78 ppm (◆), 55 ppm (○), and ≈0 ppm (●). Isobutane pressure = 0.12 atm.

observed in the rate for low inlet olefin concentrations (e.g., 50 ppm). Importantly, the H-mordenite catalyst shows no detectable activity for isobutane isomerization when very low concentrations of isobutylene are fed to the reactor.

Figure 4 shows the rate of hydrocarbon production versus time-on-stream for isobutane isomerization at 473 K for experiments in which the isobutane concentration was varied. The rate of hydrocarbon production appears to pass through a slight maximum with increasing level of isobutane in the feed stream. However, because the inlet olefin concentration has a significant effect on the rate of reaction, it is possible that some of the differences in the rate may be caused by small differences in olefin concentration for these experiments.

Reaction Scheme

Figure 5 shows a generalized scheme for isobutane isomerization over H-mordenite at 473 K. The reaction is initiated by adsorption of isobutylene on an acid site (H—B) to form an isobutyl reactive intermediate. Reactive species are represented as protonated species associated with their conjugate bases on the surface. The degree of charge distribution on the reactive intermediate is not specified here, e.g., whether the reactive intermediate is a carbenium ion (full charge transfer), a neutral surface alkoxy species, or a partially charged surface species.

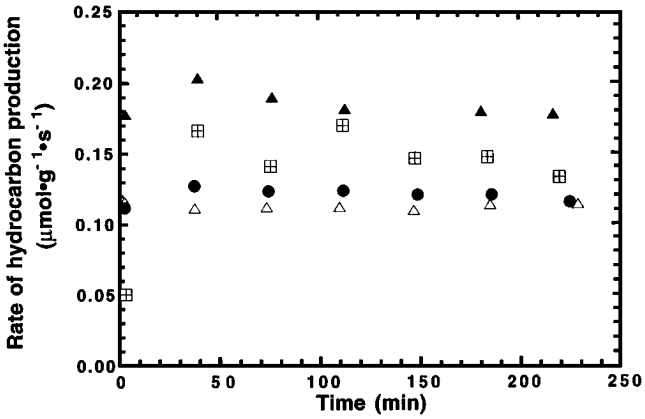

FIG. 4. Rates of total hydrocarbon production versus time-on-stream. Isobutane levels of 0.12 atm (●), 0.19 atm (▲), 0.49 atm (△), and 0.80 atm (⊞). Isobutylene concentration ≈77 ppm.

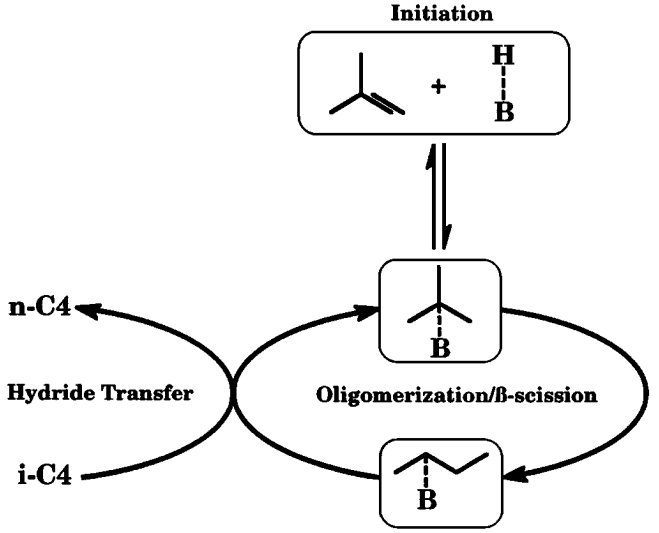

FIG. 5. Simplified reaction scheme for isobutane isomerization over H-mordenite at 473 K.

The reactive intermediate can undergo various processes, including oligomerization, β-scission, and isomerization. Eventually, an *n*-butyl reactive intermediate is formed on the surface, which can undergo hydride transfer with isobutane to form gaseous *n*-butane and an isobutyl reactive intermediate. The isobutyl reactive intermediate can then participate in further oligomerization, β-scission, and isomerization steps. Other reaction products can be produced via alternate oligomerization-cleavage pathways and hydride transfer steps.

Figure 6 outlines some of the oligomerization, β-scission, and isomerization steps involved in isobutane isomerization. Brouwer has studied and classified the relative rates of cracking and isomerization processes for carbenium ions in superacid solutions (15, 16). The oligomerization of isobutylene and an isobutyl reactive intermediate (step I) results in a trimethylpentyl reactive intermediate (2,2,4-trimethylpentyl species). According to Brouwer (16), rapid equilibration takes place among the various trimethylpentyl isomers, and these alkyl shifts are designated as type-A isomerizations. The 2,2,3-trimethylpentyl species can undergo β-scission (step II) to form an isobutyl reactive intermediate and gaseous *n*-butene. This cleavage, type-B1 cracking, is from a secondary reactive intermediate to a tertiary species. Alternatively, the 2,3,4-trimethylpentyl

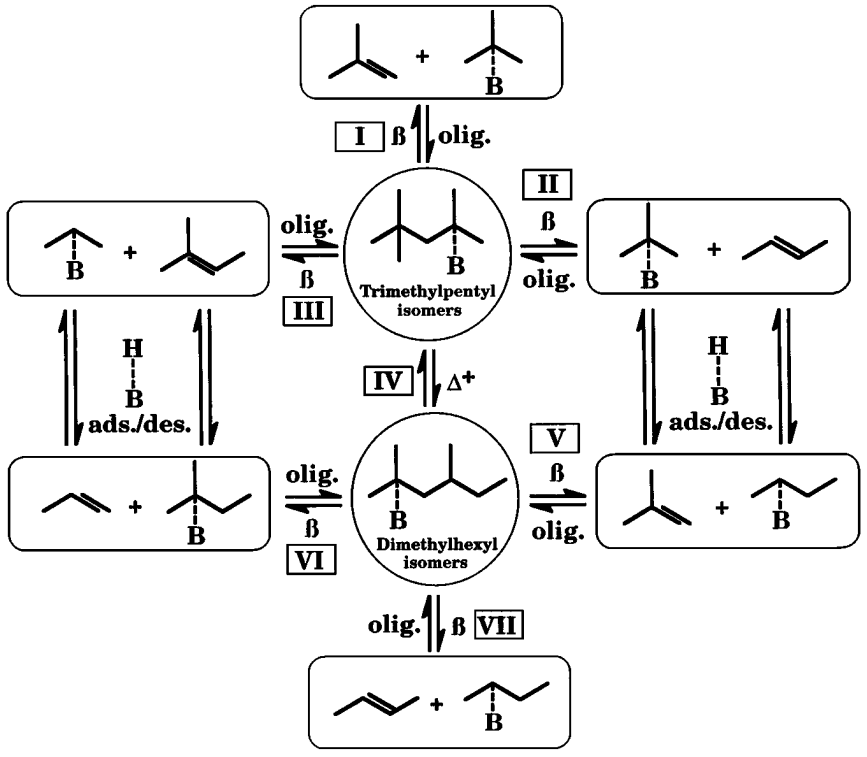

FIG. 6. Possible pathways for C_4 isomerization via C_8 intermediates. Notation: olig = oligomerization, $\beta = \beta$-scission, Δ^+ = cyclopropyl ring formation, ads./des. = adsorption and desorption.

isomer can undergo β-scission (step III) to form a propyl reactive intermediate and an isopentyl olefin. This cleavage, type-B2 cracking, is from a tertiary reactive intermediate to a secondary species. Type-A cracking, from a tertiary reactive intermediate to a tertiary species, involves cleavage of the 2,2,4-trimethylpentyl species (step I) to form isobutylene and an isobutyl reactive intermediate. Type-B isomerization, a branching rearrangement, can proceed from the trimethylpentyl species via a cyclopropyl intermediate to the dimethylhexyl species (step IV). Dimethylhexyl species can also undergo type-A isomerization to equilibrate to other dimethylhexyl isomers. The 2,4-dimethylhexyl species can undergo β-scission (step V) to form an *n*-butyl reactive intermediate and isobutylene, B2-type cracking. Alternatively, formation of the 3,3-dimethylhexyl isomer and β-scission via B1-type cracking (step VI) results in propylene and an isopentyl reactive intermediate. Type-C cracking, from a secondary reactive intermediate to a secondary species, involves cleavage of the 3,4-dimethylhexyl reactive intermediate (step VII) to form *n*-butene and an *n*-butyl reactive intermediate. The relative rates of the above reactions generally follow the trend: Hydride shift > A isomerization > A cracking > B isomerization > B1, B2 cracking > C cracking. Because Martens *et al*. (17) have observed that the rate of A cracking can be faster than A isomerization for solid catalysts, the order of the relative rates of the different cracking and isomerization steps can change, depending on the reaction conditions. As shown in Fig. 6, the reactive intermediates can desorb to produce gaseous olefins and acid sites, and olefins can adsorb on acid sites to form the corresponding reactive intermediates.

Figure 7 shows the reaction steps we have chosen to represent isobutane isomerization over H-mordenite at 473 K. This 10-step model involves oligomerization/β-scission and hydride transfer steps. Adsorption/desorption of olefins is assumed to be quasi-equilibrated, and these steps are not shown explicitly. Steps 1–5 are oligomerization/β-scission steps, where we have assumed that the isomerization of C_8 and larger reactive intermediates is rapid. Steps 1–3 are assumed to be reversible, while steps 4–5 involving intermediates larger than C_8 are assumed to be irreversible. Hydride transfer steps are presented in steps 6–10, and these steps are considered to be irreversible, because isobutane is the only alkane present in high concentrations.

The oligomerization/β-scission steps are written as the reaction of a surface reactive intermediate with a gaseous olefin. In addition, hydride transfer steps are written as reactions of surface species with gaseous isobutane. However, the gaseous species in these steps are probably weakly adsorbed in precursor states prior to reaction with the surface species. We should note that only representative isomers

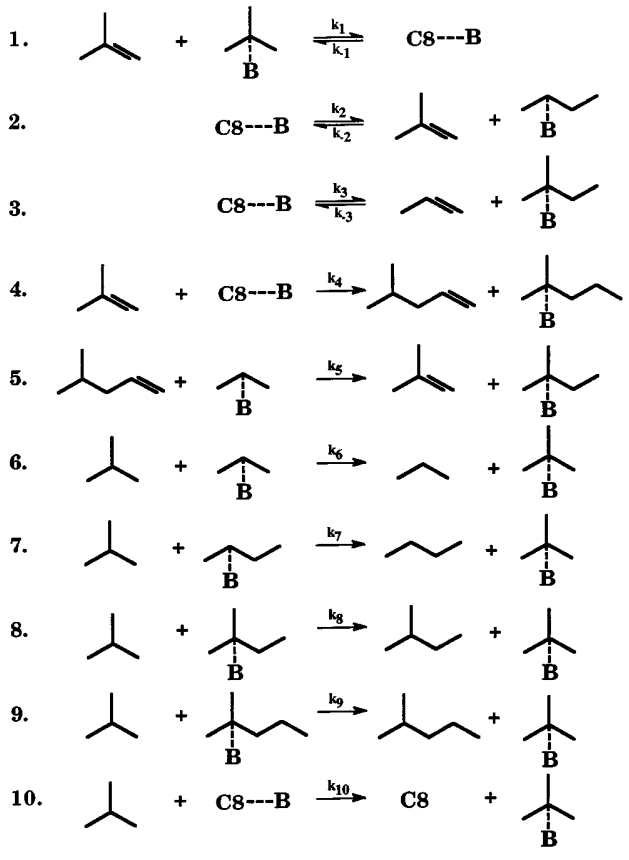

FIG. 7. Reaction scheme for isobutane isomerization and disproportionation over H-mordenite at 473 K.

are shown for the larger ($\geq C_5$) reactive intermediates and gaseous species, and we are not precluding the participation of other isomers.

Furthermore, the oligomerization/β-scission steps represent a series of steps involving oligomerization, hydride shifts, alkyl shifts, branching rearrangement, β-scission, and adsorption/desorption of the reactive intermediates. For example, the forward reaction of step 2 represents the β-scission of a C_8 reactive intermediate to form isobutylene and an *n*-butyl reactive intermediate (type-B2 cracking). The C_8 intermediate would be a dimethylhexyl isomer formed via type-B isomerization (Fig. 6, step IV) of the trimethylpentyl isomers generated by the oligomerization in step 1. Alternatively, the forward reaction of step 2 can be written as the β-scission of the trimethylpentyl reactive intermediate (Fig. 6, step II) to *n*-butene and an isobutyl reactive intermediate (type-B1 cracking), as suggested by Bearez *et al.* (18) through isotope studies of isobutane isomerization over H-mordenite. Because olefin adsorption/desorption is quasi-equilibrated and the surface concentrations of reactive intermediates are low under our experimental conditions, the formation of *n*-butene and subsequent adsorption on an acid site should be equivalent to formation of an *n*-butyl reactive intermediate. In either case, the β-scission of the C_8 reactive intermediate forms an isobutyl and an *n*-butyl species, in agreement with mechanisms proposed by others over H-mordenite (18–21).

Kinetic Model

We have constructed a kinetic model based on the reaction steps of Fig. 7 to ascertain whether the surface chemistry represented in these steps can represent the quantitative trends exhibited by the observed reaction kinetics data. A more detailed discussion of the development of this type of kinetic model is presented elsewhere (22). Briefly, the kinetic model involves estimation of rate or equilibrium constants for each step, which combined with steady state relations for the reactive intermediates, are used to calculate surface coverages and rates of consumption and formation for the reactants and products of the reaction.

We start the analysis by determining reasonable values of the kinetic parameters. We do not require a unique set of parameters, since these values will be adjusted later in the kinetic analysis. Instead, we need a feasible set of parameters, that are consistent with the surface chemistry contained in Fig. 7.

Transition state theory is used to estimate the rate constants as described in Eq. [1] (23):

$$k = \frac{k_B T}{h} e^{\Delta S^{\ddagger}/R} e^{-\Delta H^{\ddagger}/RT}, \qquad [1]$$

where k_B is the Boltzmann constant, h is the Planck constant, $\Delta S^{\ddagger}$ is the standard entropy change from the reactants to the transition state, and $\Delta H^{\ddagger}$ is the enthalpy change from the reactants to the transition state. The apparent activation energy, E_a, is approximately equal to $\Delta H^{\ddagger}$, according to the Arrhenius expression for the rate constant:

$$k = A e^{-E_a/RT}. \qquad [2]$$

Thus, the preexponential factor, A, can be estimated by

$$A = \frac{k_B T}{h} e^{\Delta S^{\ddagger}/R}. \qquad [3]$$

Equation [3] requires estimates for the standard entropies of the reacting species and the transition states. Estimates of the standard entropies of gaseous species were obtained from Stull *et al.* (24), for a standard state 473 K and 1 atm. Standard entropies of surface species were estimated by assuming that these species retained all vibrational and rotational modes but possessed none of the translational modes, as detailed in Eq. [4],

$$S_{loc} = S^{O}_{tot} - S_{trans,\,3D}, \qquad [4]$$

where S_{loc} is the local entropy of the surface species, S^{O}_{tot} is the corresponding standard entropy of the gaseous species,

and $S_{\text{trans, 3D}}$ is the translational entropy of a species with three degrees of freedom as defined in Eq. [5] (25).

$$\frac{S_{\text{trans, 3D}}}{R} = \ln\left[\frac{(2\pi m k_B T)^{3/2}}{h^3}\frac{k_B T}{P^{SS}}\right] + \frac{5}{2}, \qquad [5]$$

where m is the molecular weight, k_B is the Boltzmann constant, h is the Planck constant, T is the reaction temperature, and P^{SS} is the standard state pressure (1 atm). Loss of the rotational modes would not appreciably affect the results presented below. Changes in the entropic contributions for all surface species would scale the rate constants by a common factor, because the entropy associated with the rotational modes does not change appreciably between C_4 and C_8 hydrocarbons. The standard entropies of transition states were assumed to be equal to the local entropy of the corresponding gaseous species plus one degree of surface translational entropy, where the latter contribution is given by (25),

$$\frac{S_{\text{trans, 1D}}}{R} = \ln\left[\frac{(2\pi m k_B T)^{1/2}}{h\sqrt{C_*^{SS}}}\right] + \frac{3}{2}, \qquad [6]$$

where m is the molecular weight, k_B is the Boltzmann constant, h is the Planck constant, T is the reaction temperature, C_*^{SS} is the standard surface concentration (10^{15} molecules per cm^2).

We utilized the Evans–Polanyi correlation to express activation energies in terms of the enthalpies of reactions (25),

$$E_a = E_o + \alpha \Delta H, \qquad [7]$$

where E_a is the activation energy, E_o is the activation energy parameter for the reaction family, ΔH is the enthalpy of reaction for the given reaction step, and α is a constant for the reaction family and for simplicity was set equal to 0.5 for all reactions.

Enthalpies of the gaseous species were estimated from the heats of formation at 473 K calculated from the equations provided in Ref. (26). For the enthalpy of surface species, we adjusted the enthalpy of the gaseous species by the heat of adsorption of the various gaseous species. Through linear correlations between heats of adsorption and gas phase proton affinities (27, 28), we estimated that the heat of adsorption of 2-methyl-2-butene is ~115 kJ/mol on H-mordenite. We scaled the heats of adsorption of the various surface species from 85 kJ/mol for C_3 species to 160 kJ/mol for C_8 species, where the heat of adsorption was increased by 15 kJ/mol per additional carbon to reflect additional bonding of the larger molecules (similar to the trend reported for alkane sorption on zeolites (29, 30)). Initial values for the activation energy parameters of the reaction families, E_o, were equal to 110 kJ/mol for oligomerization/β-scission, 70 kJ/mol for hydride transfer, and 95 kJ/mol for combined oligomerization/β-scission steps, and these values were found by fitting the kinetic data using the three reaction family energies as parameters.

TABLE 2

Initial Estimates of Rate Constants for Isobutane Isomerization over H-Mordenite at 473 K

Step	k_{for}[a]	k_{rev}[a]
1	1.39E+04	4.08E−01
2	2.07E−01	2.74E+04
3	2.13E−01	1.38E+03
4	9.98E+00	—
5	4.81E+07	—
6	1.61E+00	—
7	1.99E+00	—
8	2.01E−01	—
9	9.74E+00	—
10	1.51E−02	—

[a] Units of s^{-1} or s^{-1} atm^{-1}.

Kinetic Analysis

Using the aforementioned estimates for the standard entropy changes and activation energies, values of the rate constants at 473 K were estimated for the steps presented in Fig. 7, as summarized in Table 2. These values were then used as initial guesses to fit the reaction kinetics data collected at 40 min time-on-stream. The reactor was assumed for simplicity to be a well-mixed reactor. Table 3 shows the ratios of the fitted rate constants to the initial rate constants for isobutane isomerization over H-mordenite at 473 K. The total fractional surface coverage ranged from 0.07 to 0.26 for the final rate constants.

A ratio of the fitted to the initial rate constant which is near unity indicates that the estimates for the rate constants based on the standard entropy changes and activation energies were reasonable. Values far from unity suggest that changes in the estimates for the heats of adsorption, values of E_o, and/or standard entropies are needed. For ex-

TABLE 3

Ratio (η) of Fitted to Initial Rate Constants for Isobutane Isomerization over H-Mordenite at 473 K

Step	η_{for}	η_{rev}
1	1.08E−01	3.31E−01
2	6.00E−01	3.62E+01
3	1.01E−01	4.31E−01
4	8.69E+00	—
5	2.02E−01	—
6	2.28E−01	—
7	3.85E+00	—
8	2.86E−01	—
9	1.18E+01	—
10	6.48E−01	—

ample, the small ratios for steps 5 and 6 suggest that the heat of adsorption for propylene should be increased from 85 kJ/mol. Similarly, the heat of adsorption for C_5 olefin should be increased from 115 kJ/mol as the ratios for step 8 and the reverse reaction in step 3 are smaller than unity. It appears the heat of adsorption for *n*-butene and isobutylene are not equivalent as the large value of the ratio for the reverse reaction in step 2 indicates that the heat of adsorption for *n*-butene should be lower than the estimated value of 100 kJ/mol used for isobutylene. Furthermore, the heat of adsorption of C_6 olefin should be lowered to reduce the value of the ratio in step 9. Importantly, however, all ratios of rate constants in Table 3 range between 0.1 and 40, indicating that our initial parameterization of the kinetic model is reasonable. We should note that the assumption of complete mixing within the reactor is not critical for the purposes of this paper. In particular, all of the trends predicted by our kinetic model based on a well-mixed reactor can be reproduced by a kinetic model based on a plug-flow reactor, if the rate constants for steps 4, 5, and 6 are multiplied by 0.1, 0.2, and 2, respectively.

Figure 8A shows the experimental and calculated rates of hydrocarbon production and *n*-butane production as turnover frequencies, TOF (ks^{-1}), versus the level of isobutylene fed to the H-mordenite catalyst at 473 K. The values of TOF were calculated assuming 400 μmol/g of acid sites. The H-mordenite catalyst shows no measurable activity for isobutane isomerization when no detectable isobutylene is fed to the reactor, and catalytic activity increases monotonically as the level of isobutylene fed to the reactor is increased. The fit obtained from the model appears to accurately represent the observed production rate of hydrocarbons as well as the formation of *n*-butane. Figure 8B shows the rates of hydrocarbon production and *n*-butane production versus the concentration of isobutane fed to the H-mordenite catalyst at 473 K. For the data shown, the isobutylene concentration fed to the reactor is ca 77 ppm. As the concentration of isobutane fed to the reactor is increased, it appears that rate of *n*-butane production increases over the H-mordenite catalyst, and the model appears to reproduce the experimental trend.

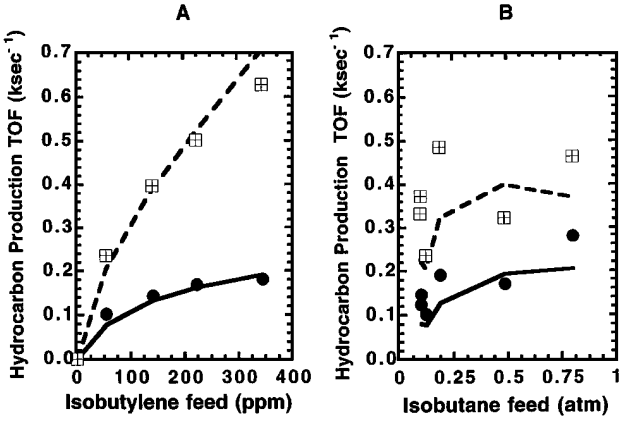

FIG. 8. Rates of total hydrocarbon production (⊞) and *n*-butane production (●) versus isobutylene feed. Solid and dashed lines represent calculated results from kinetic model. (A) Isobutane pressure = 0.12 atm. (B) Isobutylene concentration ≈77 ppm.

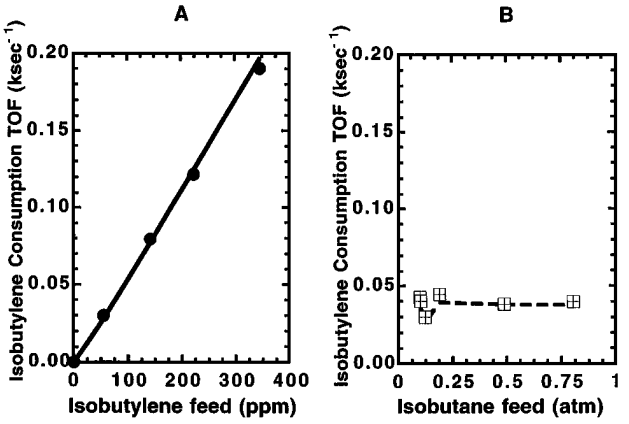

FIG. 9. A. Rates of isobutylene consumption (●) versus isobutylene feed. Solid line represents calculated results from kinetic model. Isobutane pressure = 0.12 atm. B. Rates of isobutylene consumption (⊞) versus isobutane feed. Dashed line represents calculated results from kinetic model. Isobutylene concentration ≈77 ppm.

Figure 9A shows the experimental and calculated rates of isobutylene consumption versus the level of isobutylene fed to the H-mordenite catalyst at 473 K, where the pressure of isobutane fed to the reactor is 0.12 atm. The H-mordenite catalyst consumes increasing amounts of isobutylene as the concentration of isobutylene fed to the reactor is increased, and the model appears to fit this experimental finding. Figure 9B shows the rate of isobutylene conversion versus the pressure of isobutane fed to the H-mordenite catalyst at 473 K, where the isobutylene concentration fed to the reactor is ca 77 ppm. The H-mordenite catalyst consumes approximately the same amount of isobutylene regardless of the concentration of isobutane fed to the reactor system, and the model predicts a similar trend.

Figure 10A shows the experimental and calculated rates of C_3 production versus the level of isobutylene fed to the H-mordenite catalyst at 473 K, where the pressure of isobutane fed to the reactor is 0.12 atm. The catalyst produces increasing amounts of C_3 (propane and propylene) as the amount of isobutylene fed to the reactor is increased. The model appears to predict the correct trend of C_3 production. Figure 10B shows the rate of C_3 production versus the concentration of isobutane fed to the H-mordenite catalyst at 473 K, where the isobutylene concentration fed to the reactor is ca 77 ppm. The H-mordenite catalyst produces approximately the same amount of C_3 regardless of the concentration of isobutane fed to the reactor system, and the model predicts a similar trend.

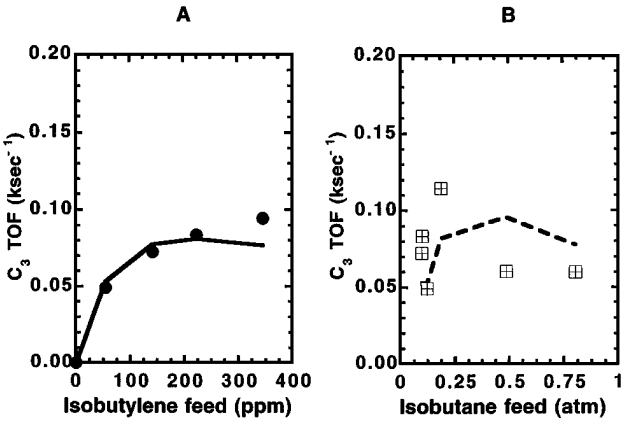

FIG. 10. A. Rates of C_3 production (●) versus isobutylene feed. Solid line represents calculated results from kinetic model. Isobutane pressure = 0.12 atm. B. Rates of C_3 production (⊞) versus isobutane feed. Dashed line represents calculated results from kinetic model. Isobutylene concentration ≈77 ppm.

Figure 11A shows the experimental and calculated rates of C_5 production versus the level of isobutylene fed to the H-mordenite catalyst at 473 K, where the pressure of isobutane fed to the reactor is 0.12 atm. The rate of C_5 production increases with increasing isobutylene concentration. Furthermore, the rate of C_5 production is approximately the same as the rate of C_3 production for low levels of isobutylene fed to the reactor; however, the rate of C_5 production is over three times the rate of C_3 production at higher levels of isobutylene fed to the reactor. Figure 11B shows the rate of C_5 production versus the concentration of isobutane fed to the H-mordenite catalyst at 473 K, where the isobutylene concentration fed to the reactor is ca 77 ppm. The H-mordenite catalyst produces approximately the same amount of C_5 regardless of the concentration of isobutane fed to the reactor system. All of the experimental trends shown in Fig. 11 are reproduced by the kinetic model.

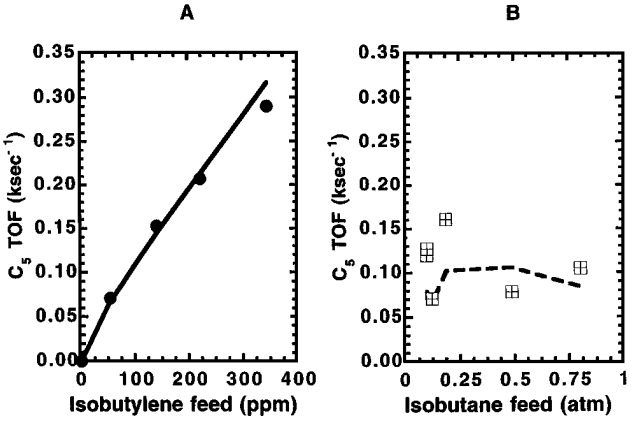

FIG. 11. A. Rates of C_5 production (●) versus isobutylene feed. Solid line represents calculated results from kinetic model. Isobutane pressure = 0.12 atm. B. Rates of C_5 production (⊞) versus isobutane feed. Dashed line represents calculated results from kinetic model. Isobutylene concentration ≈77 ppm.

Analysis of the sensitivity of the fitted rate constants can suggest which steps are more important in describing isobutane isomerization over H-mordenite. The rate constants for steps 2 and 7 are particularly sensitive. The rate constants for steps 5 and 9 are not sensitive. The remaining rate constants are moderately sensitive.

DISCUSSION

The major reaction pathways during isobutane conversion over H-mordenite at our reaction conditions are isomerization to *n*-butane and disproportionation to propane and pentane. Guisnet and Gnep (31) reported that isobutane underwent disproportionation over H-mordenite at temperatures between 523 and 623 K, and Krupina *et al.* (21) and Asuquo *et al.* (19) observed disproportionation of *n*-butane over H-mordenite at similar reaction temperatures. Yori *et al.* (5) observed disproportionation products over H-mordenite for *n*-butane isomerization at 673 K. Other work by Guisnet and co-workers (18, 20, 31–33) reported that isobutane isomerization is bimolecular and proceeds through a C_8 intermediate. Asuquo *et al.* (19) suggested that *n*-butane isomerization involved the formation of a branched C_8 intermediate, cleavage to form isobutylene and *n*-butene which readsorb prior to leaving the zeolite, and hydride transfer of the isobutyl species with the reactant to form isobutane.

The major products (C_3, *n*-C_4, and C_5) we observe are consistent with those reported by others for isobutane isomerization over H-mordenite (18, 20, 31, 33). However, others (18–21, 31, 33, 34) have observed higher rates of C_3 production than C_5 production at higher conversions or at higher reaction temperatures. For example, Krupina *et al.* (21) observed higher levels of C_3 than C_5 for *n*-butane isomerization at 623 K. However, the level of C_3 decreased while the level of C_5 remained constant when the reaction temperature was lowered to 523 K. Furthermore, equal levels of C_3 and C_5 were detected for the reaction of iso-octane over H-mordenite at 523 K (21). Hence, for our reaction conditions, the higher rate of C_5 production than C_3 formation may be a result of our lower reaction temperature. In addition, our studies were performed at low isobutane conversions (0.4–1.4%). Guisnet and Gnep (31) reported that equimolar amounts of C_3 and C_5 were produced at low isobutane conversions and more C_3 than C_5 was observed as the isobutane conversion increased. Similar product distributions are reported by Asuquo *et al.* (19) as a function of conversion for *n*-butane isomerization over H-mordenite at 523 K.

It can be seen in Figs. 8A–11A that an increase in the isobutylene feed concentration results in a higher level

of hydrocarbon production or isobutylene consumption. In the limiting case, when no detectable concentration of isobutylene is present in the feed stream, no catalytic activity is observed. Weisz (11) observed an increase in *n*-butane conversion over H-mordenite when the olefin concentration in the feed was increased. Guisnet and Gnep (31) reported that the addition of 0.7 wt% isobutylene increased by 2.5 times the initial rate of isobutane conversion.

It can be seen in Figs. 1 and 2 that hydrogen has essentially no effect on the catalyst activity or selectivity. Bearez *et al.* (20) reported that hydrogen has no influence on isobutane isomerization over H-mordenite at 623 K, except to improve the catalyst stability by reducing coke formation. These results, combined with the observation of no detectable catalytic activity when no olefins are present in the feed stream, suggest that H-mordenite displays no hydrogenation/dehydrogenation activity at our reaction conditions. Thus, isobutylene present in the feed is involved in the initiation as well as the oligomerization reactions over H-mordenite.

As the concentration of isobutylene fed to catalyst increases, the selectivity towards *n*-butane decreases (see Fig. 8A). In addition, an increase in the deactivation rate is observed as the level of isobutylene is increased (see Fig. 3). Thus, an increased level of isobutylene results in increased *n*-butane production, but also increased side reactions such as coking and oligomerization/β-scission reactions which lead to C_3, C_5, and C_6 products. This behavior is caused by a higher fractional coverage of the surface by adsorbed hydrocarbon species at the higher levels of isobutylene.

Since the catalytic cycles presented in Fig. 7 adequately describe the observed kinetics for isobutane conversion over H-mordenite at 473 K, we may use these cycles to probe the relative rates of the various processes that take place on the catalyst surface. The forward and reverse rates of oligomerization/β-scission for steps 1 and 2 appear to be an order of magnitude faster than hydride transfer reactions for low pressures of isobutane ($\sim$0.12 atm), and about twice the rate of hydride transfer to form *n*-butane (step 7) at higher isobutane pressures ($\sim$0.80 atm). The forward and reverse rates of oligomerization/β-scission for step 3 are about twice the rate of hydride transfer to form *n*-butane (step 7) for low pressures of isobutane ($\sim$0.12 atm). At higher isobutane pressures ($\sim$0.80 atm), the forward rate of step 3 is $\sim$2 times slower than the rate of hydride transfer to form *n*-butane (step 7) and about the same as the rates of hydride transfer to form propane (step 6) and pentane (step 8). For higher isobutane pressures ($\sim$0.80 atm), the reverse rate of step 3 is $\sim$10 times slower than the rate of hydride transfer to form *n*-butane (step 7) and $\sim$4 times slower than the rate of hydride transfer to form propane (step 6) and pentane (step 8). The rate of β-scission of the C_8 reactive intermediate to form an isobutyl and an *n*-butyl species (forward rate of step 2) is $\sim$5 times faster than the rate of β-scission of the C_8 reactive intermediate to form a propyl and a pentyl species (forward rate of step 3) and $\sim$10% slower than the reverse rate of step 1. These results are in agreement with the observations by Brouwer (16) that type A cracking is faster than other cracking pathways (types B1 and B2).

Isobutane appears to have a smaller effect than isobutylene on the rates of hydrocarbon production (see Figs. 8B–11B). Only for *n*-butane production (Fig. 8B) does an increase in the concentration of isobutane result in a higher rate of production. This behavior results from a change in the reversibility of the oligomerization steps with increasing isobutane pressure. In particular, for isobutylene outlet concentrations of 5 ppm (corresponding to inlet isobutylene concentrations of 50 ppm), the β-scission of the C_8 reactive intermediate to C_3 and C_5 species (step 3) is reversible at lower isobutane pressure (0.12 atm), while as the isobutane pressure increases to 0.80 atm, step 3 becomes essentially irreversible. This departure from reversibility reflects a decrease in the surface concentration of the C_5 reactive intermediate with increasing isobutane pressure. The surface concentration of *n*-butyl species does not decrease as much as the other surface intermediates because the *n*-butyl reactive intermediate is generated by faster β-scission (step 2) than step 3.

While it is not feasible to derive an analytical expression for the full reaction mechanism presented in Fig. 7, a rate expression for isobutane isomerization can be obtained based upon a simplified reaction scheme. This simplified reaction scheme involves oligomerization of isobutylene and an isobutyl reactive intermediate to form a C_8 species (step 1, Fig. 7), β-scission of the C_8 species to give isobutylene and an *n*-butyl reactive intermediate (step 2, Fig. 7), hydride transfer of the *n*-butyl reactive intermediate with isobutane (step 7, Fig. 7), and quasi-equilibrated adsorption/desorption of isobutylene. For these reaction steps, the rate of isobutane isomerization can be described by Eq. [8],

$$R_{\text{isom}} = \frac{k_1 k_2 k_7 K_{i=} P_i P_{i=}^2}{k_1 K_{i=} P_{i=}^2 (k_2 + k_7 P_i + k_{-2} P_{i=}) + (1 + K_{i=} P_{i=})(k_2 k_7 P_i + k_{-1} k_7 P_i + k_{-1} k_{-2} P_{i=})}, \quad [8]$$

where R_{isom} is the rate of isobutane isomerization, $K_{i=}$ is the equilibrium constant for isobutylene adsorption (7.7×10^3 for a reference state of 1 atm and a reaction temperature of 473 K), k_i and k_{-i} are the forward and reverse rate constants for an *i*th step obtained from Tables 2 and 3 for the model presented in Fig. 7, P_i and $P_{i=}$ are the pressures of isobutane and isobutylene, respectively, in atm.

As the outlet isobutylene concentration increases from 5 to 40 ppm (corresponding to inlet isobutylene concentrations of 50 to 350 ppm) at a constant isobutane pressure of 0.12 atm, the dominant terms in the denominator of

the rate expression in Eq. [8] become $K_{i=}P_{i=}$, $k_{-1}k_{-2}P_{i=}$, and $k_{-2}P_{i=}$. Under these conditions, the rate expression reduces to

$$R_{\text{isom}} = \frac{k_7 K_{i=} K_1 K_2 P_i P_{i=}}{1 + K_{i=}P_{i=} + K_{i=}K_1 P_{i=}^2}. \quad [9]$$

The rate of isomerization in Eq. [9] depends on the equilibrium constants for steps 1 and 2, the rate constant for step 7, the equilibrium constant for isobutylene adsorption, as well as the pressures of isobutane and isobutylene. In agreement with the observed trend in Fig. 8A, Eq. [9] predicts a higher rate of isomerization with increasing concentration of isobutylene at constant isobutane pressure.

As the isobutane pressure increases from 0.10 to 0.80 atm at a constant outlet isobutylene concentration of 5 ppm, the dominant terms in the denominator of the rate expression in Eq. [8] become $k_2k_7P_i$, $k_1k_7P_i$ and $k_{-1}k_{-2}P_{i=}$. Under these conditions, the rate expression reduces to

$$R_{\text{isom}} = \frac{k_1 k_2 k_7 K_{i=} P_i P_{i=}^2}{(k_2k_7 + k_{-1}k_7)P_i + k_{-1}k_{-2}P_{i=}}. \quad [10]$$

The rate of isomerization in Eq. [10] depends on the forward and reverse rate constants for steps 1 and 2, the rate constant for step 7, the equilibrium constant for isobutylene adsorption, as well as the pressures of isobutane and isobutylene. In agreement with the observed trend in Fig. 8B, Eq. [10] predicts a higher rate of isomerization with increasing isobutane pressure (0.10–0.80 atm) at constant outlet isobutylene concentration of 5 ppm. It is apparent from Eq. [10] that the terms $k_2k_7P_i$ and $k_1k_7P_i$ would become larger than $k_1k_{-2}P_{i=}$ for higher isobutane and/or lower isobutylene outlet concentrations. In this regime, the rate expression reduces to

$$R_{\text{isom}} = \frac{k_1 k_2 K_{i=} P_{i=}^2}{k_2 + k_{-1}}. \quad [11]$$

The rate of isomerization in Eq. [11] depends on the rate constants for steps 1 and 2, the equilibrium constant for isobutylene adsorption, as well as the pressure of isobutylene. Under these conditions, the rate expression exhibits no dependence on isobutane pressure.

From the rate expressions described above, it is apparent that the reversibility of the oligomerization/β-scission steps dictates the form of the rate expression. In general, higher isobutylene concentrations result in more equilibrated oligomerization/β-scission steps, while higher isobutane pressures decrease the reversibility of the oligomerization/β-scission steps for our reaction conditions. Thus, at higher isobutane pressures for a constant isobutylene concentration of 5 ppm, the oligomerization/β- scission steps become more irreversible, and the rate of isomerization follows Eq. [10] and for subsequently higher isobutane pressures follows Eq. [11]. Accordingly, as the oligomerization/β-scission steps become more irreversible at higher isobutane pressures, the rate of isobutane isomerization becomes essentially independent of the isobutane pressure. At higher isobutylene concentrations for a constant isobutane pressure of 0.12 atm, the oligomerization/β-scission steps are more reversible and the rate of isomerization follows expression of Eq. [9]. Under these conditions, the rate of isomerization depends on the pressures of both isobutane and isobutylene.

It is useful to note that reactive intermediates appear to follow reaction pathways similar to those exhibited by known carbenium ion chemistry. As the concentrations of reactive intermediates increase, more oligomerization and β-scission reactions occur and result in increased production of hydrocarbons. Using a simple kinetic model we are able to simulate the observed kinetic data for isobutane isomerization over H-mordenite at 473 K. The calibration of this kinetic model provides a quantitative description of the surface chemistry for isobutane conversion over H-mordenite, and this model may provide a framework for comparison of isobutane conversion over other acidic catalysts systems near our reaction conditions. In particular, we have extended this work to examine isobutane isomerization over sulfated zirconia (35). Having quantified in the present study the kinetics for isobutane isomerization over H-mordenite for the case where olefins were generated in the feed, we are able to extend the analysis to the case of sulfated zirconia where olefins are generated *in situ* by the catalyst during isobutane isomerization.

CONCLUSIONS

Reaction kinetics studies were conducted of isobutane conversion over H-mordenite at 473 K using a system comprised of two reactors connected in series. The first reactor was loaded with Pt/Sn catalyst and controlled the olefin concentration in the feed to the second reactor containing H-mordenite by varying the dehydrogenation–hydrogenation equilibrium between butanes and butenes. A kinetic model has been developed to describe isobutane isomerization over H-mordenite at 473 K. The kinetic model contains reaction steps involving olefin adsorption/desorption, oligomerization/β-scission (where the isomerization of C_8 and larger reactive intermediates is rapid), and hydride transfer. For our reactions conditions, the rates of oligomerization/β-scission steps involving C_4 species are faster than the rates of hydride transfer. The presence of isobutylene increases the rates of isobutane conversion, most likely by increasing the surface concentration of reactive intermediate species. However, an increased level of isobutylene results in higher rates of other reactions such as coking and oligomerization/β-scission which lead to production of C_3, C_5, and C_6 species. For our reaction conditions, higher isobutylene concentrations

result in more equilibrated oligomerization/β-scission steps, while higher isobutane pressures decrease the reversibility of the oligomerization/β-scission steps. The reactive intermediates appear to follow reaction pathways similar to those exhibited in known carbenium ion chemistry.

ACKNOWLEDGMENTS

This work was supported by funds provided by the Office of Basic Energy Sciences of the U.S. Department of Energy. We also acknowledge G. B. McVicker for his suggestions regarding the experimental approach of using two reactors connected in series.

REFERENCES

1. Arata, K., *Adv. Catal.* **37**, 165 (1990).
2. Yamaguchi, T., *Appl. Catal.* **61**, 1 (1990).
3. Hsu, C. Y., Heimbuch, C. R., Armes, C. T., and Gates, B. C., *J. Chem. Soc., Chem. Comm.* 1645 (1992).
4. Yaluris, G., Larson, R. B., Kobe, J. M., González, M. R., Fogash, K. B., and Dumesic, J. A., *J. Catal.* **158**, 336 (1996).
5. Yori, J. C., Luy, J. C., and Parera, J. M., *Appl. Catal.* **46**, 103 (1989).
6. Chen, F. R., Courdurier, G., Joly, J., and Vedrine, J. C., *J. Catal.* **143**, 616 (1993).
7. Garin, F., Andriamasinoro, D., Abdulsamad, A., and Sommer, J., *J. Catal.* **131**, 199 (1991).
8. Ward, D. A., and Ko, E. I., *J. Catal.* **150**, 18 (1994).
9. Liu, H., Adeeva, V., Lei, G. D., and Sachtler, W. M. H., *J. Mol. Catal. A: Chem.* **100**, 35 (1995).
10. Pines, H., and Wackher, R. C., *J. Am. Chem. Soc.* **68**, 595 (1946).
11. Weisz, P. B., *Chemtech.* 498 (1973).
12. Tábora, J. E., and Davis, R. J., *J. Catal.* **162**, 125 (1996).
13. Fogash, K. B., Hong, Z., Kobe, J. M., and Dumesic, J. A., *J. Catal.* submitted.
14. McVicker, G. B., personal communication.
15. Brouwer, D. M., and Hogeveen, H., *in* "Progress in Physical Organic Chemistry" (A. J. Streitwieser and R. W. Taft, Eds.), p. 179, Wiley, New York, 1972.
16. Brouwer, D. M., *in* "Chemistry and Chemical Engineering of Catalytic Processes" (R. Prins and G. C. A. Schuit, Eds.), p. 137, Sijthoff & Noordhoff, Alphen a/d Rijn, 1980.
17. Martens, J. A., Jacobs, P. A., and Weitkamp, J., *Appl. Catal.* **20**, 239 (1986).
18. Bearez, C., Avendano, F., Chevalier, F., and Guisnet, M., *Bull. Soc. Chim. Fr.* **3**, 346 (1985).
19. Asuquo, R. A., Eder-Mirth, G., and Lercher, J. A., *J. Catal.* **155**, 376 (1995).
20. Bearez, C., Chevalier, F., and Guisnet, M., *React. Kinet. Catal. Lett.* **22**, 405 (1983).
21. Krupina, N. N., Proshurnin, A. L., and Dorogochinskii, A. Z., *React. Kinet. Catal. Lett.* **32**, 135 (1986).
22. Yaluris, G., Reskoske, J. E., Aparicio, L. M., Madon, R. J., and Dumesic, J. A., *J. Catal.* **153**, 54 (1995).
23. Laidler, K. J., "Chemical Kinetics," Harper & Row, New York, 1987.
24. Stull, D. R., Westrum, E. F., Jr., and Sinke, G. C., "Chemical Thermodynamics of Organic Compounds," Wiley, New York, 1969.
25. Dumesic, J. A., Rudd, D. F., Aparicio, L. M., Rekoske, J. E., and Treviño, A. A., "The Microkinetics of Heterogeneous Catalysis," Amer. Chem. Soc., Washington, DC, 1993.
26. Yaws, C. L., "Thermodynamic and Physical Property Data," Gulf Publ., Houston, 1992.
27. Chen, D. T., Zhang, L., Yi, C., and Dumesic, J. A., *J. Catal.* **146**, 257 (1994).
28. Lee, C., Parrillo, D. J., Gorte, R. J., and Farneth, W. E., *J. Am. Chem. Soc.* **118**, 3262 (1996).
29. Haag, W. O., *in* "Catalysis by Zeolites, in Zeolites and Related Microporous Materials: State of the Art 1994" (J. Weitkamp *et al.*, Eds.), p. 1375, Elsevier, Amsterdam, 1994.
30. June, R. L., Bell, A. T., and Theodorou, D. N., *J. Phys. Chem.* **94**, 1509 (1990).
31. Guisnet, M., and Gnep, N. S., *Appl. Catal. A: Gen.* **146**, 33 (1996).
32. Guisnet, M., Andy, P., Gnep, N. S., Benazzi, E., and Travers, C., *J. Chem. Soc., Chem. Commun.*, 336 (1985).
33. Hilaireau, P., Bearez, C., Chevalier, F., Perot, G., and Guisnet, M., *Zeolites* **2**, 69 (1982).
34. Asuquo, R. A., Eder-Mirth, G., Seshan, K., Pieterse, J. A. Z., and Lercher, J. A., *J. Catal.* **168**, 292 (1997).
35. Fogash, K. B., Hong, Z., and Dumesic, J. A., *J. Catal.* submitted.